Dynamical basis for Koba-Nielsen-Olesen scaling and its violation

D. C. Hinz and C. S. Lam
Department of Physics, McGill University, Montreal, Quebec, Canada H3A 2T8
(Received 21 June 1985)

We discuss a class of dynamical models motivated by Koba-Nielsen-Olesen (KNO) scaling and phase-space considerations. These modified phase-space models (MPSM's) generalize some of the existing models and provide them with a dynamical basis. Multiplicity distributions in MPSM's can be obtained by solving an appropriate evolution equation, from which kinematical KNO-scaling violations before the asymptotic scaling energy is reached can be calculated. Possible causes for dynamical KNO-scaling violations are also discussed.

I. INTRODUCTION

Koba-Nielsen-Olesen (KNO) scaling[1] for multiplicity distributions is probably the best scaling law we have. It works remarkably well for a great variety of reactions over a wide range of energies.[2-4] If interpreted correctly the apparent violation of KNO scaling observed at the CERN $S\bar{p}pS$ collider at $\sqrt{s}=540$ GeV (Ref. 5) will also disappear.[14]

There is a large number of models proposed to explain KNO scaling, approximate KNO scaling, or merely the associated large multiplicity fluctuations.[6-10] The latter is achieved in a class of models[7,8] by the incoherent superposition of narrow distributions such as the Poisson distribution. KNO scaling is not guaranteed in this approach unless additional ingredients are introduced. Otherwise approximate KNO scaling will simply emerge as a result of the numerical calculations.

Another class of models is constructed in such a way that KNO scaling emerges from the very beginning. Examples of this class of model are the stochastic cell model[6] and the three-fireball model.[10]

We shall adopt the point of view that the excellence of the KNO-scaling law should be treated seriously and should be utilized as a guide for our search for the underlying dynamical mechanisms for strong-interaction reactions. Our goal is to make a systematic study of the problem in order to find the most general dynamical scheme capable of predicting KNO scaling. Once this is done one would also understand how KNO-scaling violations can be achieved. We cannot claim to be completely successful in that goal, but we have found a large enough class of dynamical models to be able to begin a systematic dynamical study using KNO scaling as an input. To this end we note that the probability $P_n(\bar{n})$ for producing n particles at an incoming c.m. energy $\sqrt{s}$ that yields an average multiplicity $\bar{n}(s)$ satisfies the evolution equation[11]

$$2\frac{dP_n}{dx}=f_{n-1}P_{n-1}-f_nP_n \tag{1}$$

in at least two cases. If $P_n(\bar{n})$ is given by a Poisson distribution, then $x=2\bar{n}$ and $f_n=1$. If $P_n(\bar{n})$ obeys KNO scaling, then (1) is again satisfied in the KNO limit $n\gg1$, $\bar{n}\gg1$, $z=n/\bar{n}$ fixed.[11] In that case we should take $x=2\ln(\bar{n})$ and $f_n=n$. We shall adopt the convention in (1) and below that $P_n=0$ if $n<0$.

For the Poisson distribution, Eq. (1) may be interpreted as follows. Let the probability for emitting an additional particle as we change the energy from s to $s+ds$ be given by $dx/2$ for some $x(s)$. Then the rate of change of $P_n(\bar{n})$ is given by the right-hand side of (1), with the first term describing the gain in P_n due to the emission of an additional particle when $n-1$ particles are already present, and the second describing the loss in P_n due to the emission of an additional particle in the presence of n of them. Thus this equation describes the independent emission from a single source, as is depicted by the multiperipheral chain in Fig. 1. The relaxation $x=2\bar{n}$ is a consequence of Eq. (1).

By the same token Eq. (1) can be interpreted similarly[11] for KNO distributions in the KNO limit. Since now $f_n=n$, we must have n sources participating in the emission of particles. This means that every particle present must be capable of acting as a source and this naturally suggests a picture given by the multichain diagram depict-

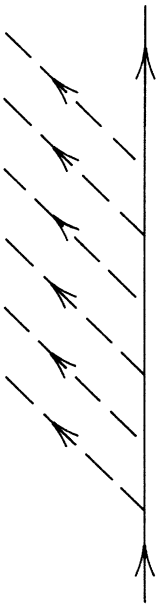

FIG. 1. A multiperipheral diagram.

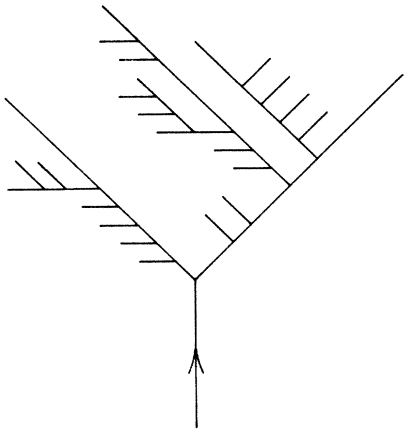

FIG. 2. A multichain diagram with ϕ^3 vertices.

ed in Fig. 2. Again $x=2\ln(\bar{n})$ is a consequence of Eq. (1).

Chain models have been studied previously by other authors.[12] We shall consider here a particular version of such a model which is largely based on phase-space considerations. It is in fact a phase-space model motivated by KNO scaling that is modified minimally to allow for an arbitrary average multiplicity function $\bar{n}(s)$. We shall refer to this model as the modified phase-space model (MPSM).

We shall define and study this model for a one-channel problem in Sec. II. Initially we shall discuss the case when the dynamics is described by an $l+2=3$ prong vertex as is depicted in Fig. 2, but later on the cases for other l's are also considered. Multichannel generalizations are straightforward and will be discussed briefly at the end of that section. We shall show that if the energy is sufficiently large, then $P_n(\bar{n})$ given by the MPSM satisfies Eq. (1) with $f_n=n$ for all n, and not only so for $n\gg 1$. In Sec. III we discuss the solution of Eq. (1), which is obviously unique once an initial condition (at some fixed $x=x_0$) is given. If $P_n(\bar{n}(x_0))=\delta_{nk}$, then $P_n(\bar{n}(x))$ is given by a function G_n^k which approaches a Γ distribution in z in the KNO limit. These Γ distributions have integral powers in z if $l=1$, but have rational powers if $l>1$. This solution corresponds to the initial production of k off-shell clusters, which subsequently decay according to the multichain dynamics depicted in Fig. 2. The solution for the case of a mixture of several initial clusters will also be discussed. We will also discuss in Sec. III an example of the two-channel case. In general the solution for this case cannot be found analytically, but we can obtain partial results for special cases and through them we see that the multichannel results could be quite different from the one-channel result discussed above.

Section IV contains an application of the one-channel analysis to $\bar{p}p$ multiplicity distributions and a discussion of the various origins of KNO-scaling violations.

II. THE MODIFIED PHASE-SPACE MODEL

It is well known that the d-dimensional n-particle phase-space factor

$$\rho^{(d)}(S\to 123\cdots n)=\int\left[\prod_{i=1}^{n} d^d k_i\,\delta(k_i^2-m_i^2)\theta(k_i^0)\right]\times\delta^d\left[k_s-\sum_{i=1}^{n}k_i\right] \tag{2}$$

can be decomposed into phase-space factors for a fewer number of particles via the formula

$$\rho(S\to 123\cdots n)=\int\rho(S\to A_1A_2\cdots A_k)\prod_{j=1}^{k}\rho(A_j\to i_1i_2\cdots i_{n(j)})\times dm^2(A_j)\,. \tag{3}$$

This formula, valid for any d, can be represented graphically by Fig. 3. In particular, repeated use of (3) allows us to decompose an n-body phase-space factor into two-body phase-space factors. The latter is given in two and four dimensions by

$$\rho^{(4)}(S\to AB)=\frac{\pi}{2}\frac{\sqrt{\lambda}}{m_s^2},\quad \rho^{(2)}(S\to AB)=\frac{1}{2\sqrt{\lambda}}\,, \tag{4}$$

where

$$\lambda=[(m_s^2-m_A^2-m_B^2)^2-4m_A^2m_B^2]^{1/2}\,. \tag{5}$$

Phenomenologically the transverse momenta $k_\perp$ of the produced particles are generally much smaller than the longitudinal momenta $k_\parallel$; therefore, the appropriate phase-space factor to use is the two-dimensional one. In this region $m_s\gg m_A,m_B$, for the reaction $S\to A+B$, and $\rho^{(2)}$ is well approximated by $1/2m_s^2$. However we must be cautious in using the two-dimensional phase-space formula in the region where $k_\perp$ is of the same order as $k_\parallel$. Since transverse and longitudinal momenta are of the same order in this region, we must take a smooth transi-

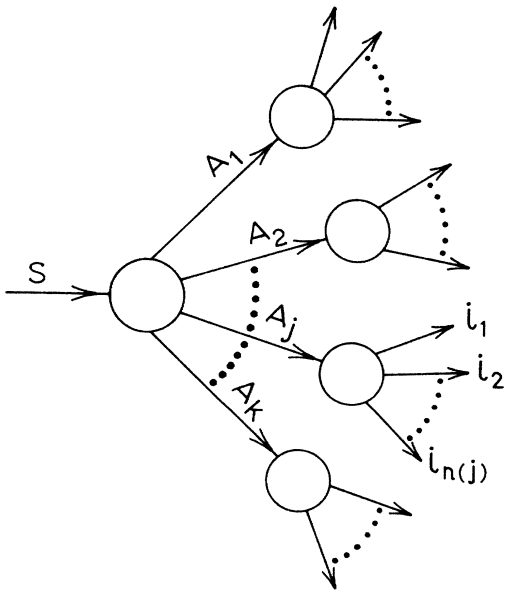

FIG. 3. A diagram illustrating the phase-space decomposition of Eq. (3).

tion from two-dimensional to four-dimensional phase-space factors. Now in this region, $m_s \sim m_A + m_B$, the function in (5) vanishes. The two-dimensional phase-space factor $\rho^{(2)}$ goes to infinity while the four-dimensional phase-space factor $\rho^{(4)}$ goes to zero. The correct phase-space factor in this region is then presumably somewhere between zero and infinity, and the exact form will depend on the details of the $k_\perp$ and the $k_\parallel$ distributions in that region. For the sake of simplicity, we shall take it to be finite and given by the two-dimensional asymptotic form given above. Thus we assume the effective two-body phase-space factor appropriate to the present problem to be

$$\rho(S \to AB) = \frac{1}{2m_s^2}\theta(m_s - m_A - m_B) . \tag{6}$$

As we shall see below, the functional form in (6) for $\rho(S \to AB)$ actually does not matter as long as it is given by a function of m_s^2 satisfying the θ-function threshold constraint.

The modified phase-space model (MPSM) is constructed below. For simplicity we shall describe in detail only the one-channel case whose dynamics is described by an effective ϕ^3 vertex. Generalization to other vertices and the inclusion of many channels are straightforward and will be discussed briefly at the end of this section.

The MPSM is constructed as follows.

(i) Draw all topologically distinct branching-type tree diagrams corresponding to a ϕ^3 vertex. Two such diagrams are topologically distinct if one cannot be obtained from another by a combination of permutations of vertices. By a permutation of vertex we mean the permutation of the two lines emerging from the vertex together with their associated tree structures. The symmetry factor (F_S) for such a diagram is defined to be the number of permutations which reproduces exactly the same diagram. We shall also use the terminology of geometrically distinct diagrams. Two diagrams obtained from one another by permutation of vertices are considered to be geometrically distinct as long as they are not identical. Thus for a diagram with v vertices, the number of geometrically distinct diagrams that are topologically identical is $2^v/F_S$.

(ii) For each toplogically distinct diagram, use Eq. (3) to decompose the phase-space factor according to this diagram, and use Eq. (6) for the two-body phase space factor. Dynamics is introduced by allowing in addition a wave-function factor $2m^2 v(m^2)$ for each form-factor-propagator combination, where m is the off-shell mass of that propagator, $v(m^2)$ is defined in such a way that it is the product of the two-body phase-space factor (6) and the newly introduced wave-function factor. Finally, we must as usual divide this diagram by its symmetry factor F_S. After summing up all the topologically distinct diagrams with n final particles, the resulting expression will be denoted by $\tilde{P}_n$.

Now $\tilde{P}_n$ would essentially have been the probability of producing n particles if the tree diagrams respected unitarity. Since they do not and since we are unwilling to calculate loop diagrams, unitarity, or rather probability conservation in the present context, must be enforced by hand in much the same that is done for the Altarelli-Parisi equation. We shall show below that $\tilde{P}_n$ satisfies the relation

$$2\frac{d\tilde{P}_n}{dx} = (n-1)\tilde{P}_{n-1} , \tag{7}$$

where

$$dx(m^2) = v(m^2)dm^2 . \tag{8}$$

It is clear that this equation does not respect probability conservation,

$$\sum_n P_n = 1 , \tag{9}$$

because the branching diagrams describe creation of particles through branching but fail to account for the loss of the initial particles that branched. We must therefore modify (7) by introducing a loss term so that (9) is satisfied. The resulting probability of producing n particles now satisfies the evolution equation

$$2\frac{dP_n}{dx} = (n-1)P_{n-1} - nP_n , \tag{10}$$

which is nothing but Eq. (1) with $f_n = n$, valid however for arbitrary n. In this way the branching diagrams $\tilde{P}_n$ act like a "potential" to drive the final unitarized probability P_n. By multiplying (10) on both sides by n and summing over all n it is easy to show that the function $x(m^2)$ is related to the average multiplicity $\bar{n}(m^2)$ by the relation

$$x(m^2) = 2\ln\bar{n}(m^2) . \tag{11}$$

Now it remains to show that Eq. (7) is true. For this purpose recall rules (i) and (ii) above for $\tilde{P}_n$. Using the variable x defined in (8), we obtain simply

$$\tilde{P}'_n = (1/F_S)\int dx_1 dx_2 dx_3 \cdots dx_l \equiv (1/F_S)\tilde{Q}_n , \tag{12}$$

where $\tilde{P}'_n$ denotes the contribution from a particular diagram whereas the unprimed expression $\tilde{P}_n$ is used to denote the sum of all n particle diagrams. In (12) there are as many x integrations as there are internal propagators. The limits of the x integrations are determined from Eq. (8) and the mass-threshold θ function in (6).

For example, the F_S factors for diagrams A,B,C,D,E in Fig. 4 are, respectively, 4,2,8,8,2, and the $\tilde{Q}'_n$ function for each of A,B,C are $\int dx_1 dx_2 dx_3$. Although these three integrals appear to be the same, actually they are not because the three diagrams have different structures and therefore different boundaries in the (x_1,x_2,x_3) space.

There are two basic ingredients involved in showing (7): one is phase space and the other is topological. We start with the phase-space consideration. Assume for the sake of simplicity the on-shell mass to be zero and $\bar{n}(0)=1$, so that $x(0)=0$. This assumption for $\bar{n}$ is not critical at all for the following analysis. Now for a two-body decay $S \to A+B$, the boundary for the x_A, x_B integrations is determined by $m_A \geq 0$, $m_B \geq 0$, and $m_s \geq m_A + m_B$. The first two conditions correspond to $x_A \geq 0$ and $x_B \geq 0$. To study the last condition let us consider two special cases.

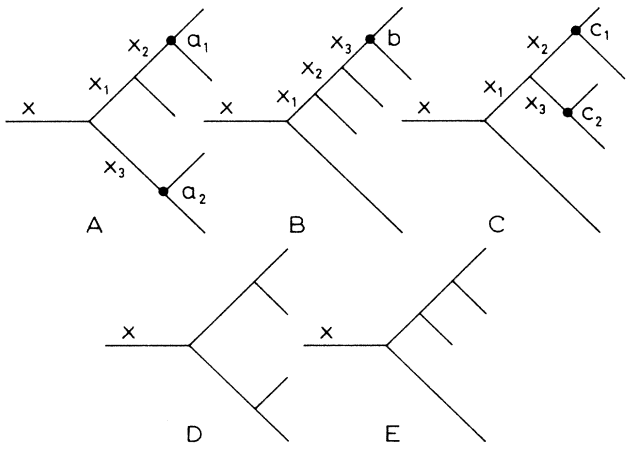

FIG. 4. Topologically distinct diagrams for $n=5$ and 4.

(1) Suppose

$$\bar{n}(m^2)=[1+\ln(m^2+1)]^{\alpha} .$$

Then (11) implies

$$x=2\alpha\ln[1+\ln(m^2+1)]$$

and (8) implies

$$v(m^2)=2\alpha/(m^2+1)[1+\ln(m^2+1)] .$$

Thus

$$m=[\exp(e^{x/2\alpha}-1)-1]^{1/2}$$

and the boundary $m_s=m_A+m_B$ maps into

$$[\exp(e^{x_s/2\alpha}-1)-1]^{1/2}$$
$$=[\exp(e^{x_A/2\alpha}-1)-1]^{1/2}+[\exp(e^{x_B/2\alpha}-1)-1]^{1/2} .$$

In particular, when $x_s \gg 2\alpha$, $m_A=0$ maps into $x_A=0$ and $x_B=x_s$, while $m_A=m_B$ maps into

$$x_A=x_B\simeq x_s-2\alpha\, e^{-x_s/2\alpha}\{2\ln 2-3\exp[-(e^{x_s/2\alpha}-1)]\} .$$

For $x_s \gg 2\alpha$, the region in (x_A,x_B) space is practically a square with length x_s on each side.

(2) Suppose $\bar{n}(m^2)=(m^2+1)^{\alpha}$. Then $x=2\alpha\ln(m^2+1)$ and $v(m^2)=2\alpha/(m^2+1)$. Hence $m=[\exp(x/2\alpha)-1]^{1/2}$ and the boundary $m_s=m_A+m_B$ maps into

$$[\exp(x_s/2\alpha)-1]^{1/2}=[\exp(x_A/2\alpha)-1]^{1/2}$$
$$+[\exp(x_B/2\alpha)-1]^{1/2} .$$

For $x_s \gg 2\alpha$, $m_A=0$ maps into $x_A=0$ and $x_B=x_s$, while $m_A=m_B$ maps into $x_A=x_B\simeq x_s-2\alpha(2\ln 2-3\,e^{-x_s/2\alpha})$. Once again the region of integration is almost a square if $x_s \gg 2\alpha$.

The conclusion of this analysis is the following. The integration region in (x_A,x_B) space is practically a square if $x \gg 4\alpha\ln 2$, and if the on-shell masses are neglected. When x_s is decreased, the phase space shrinks. It shrinks more for larger α, and it shrinks more in case (2) than in case (1). In other words, the faster the average multiplicity $\bar{n}(m^2)$ grows with m, the more the phase space will shrink. It is also important to note that the shrinkage occurs more in the region where $m_A=m_B$ than when one particle is on shell. Thus it has the effect of discouraging the decay to two off-shell particles compared to the decay to one on-shell and one off-shell particle. This effect is more prominent the faster $\bar{n}(m^2)$ rises with m. Moreover, finite on-shell masses also have the effect of cutting down the phase space of high-multiplicity events and thereby decreasing their probabilities for occurrence. In addition, since $\bar{n}(m^2)/m$ approaches zero for large m, this effect is more pronounced at low energies than at high energies.

To illustrate these features the phase-space boundaries for pp interactions where $\bar{n}(m^2)=0.88+0.44\ln(s)+0.118\ln^2(s)$, and for e^+e^- annihilations where $\bar{n}(s)=2s^{1/4}$, are plotted in Fig. 5 for two energies: $\sqrt{s}=540$ and 30 GeV. To make comparison easier, these boundaries are displayed in the y variables, where y_A (y_B) is defined to be a linear function of x_A (x_B) in such a way that $(y_A,y_B)=(0,1)$ and (1,0) are points on the phase-space boundary.

For the rest of this section we shall assume the energy to be so large that the two-body phase space may be approximated by a square in the x variables. Consider a linear chain with r propagators splitting into two diagrams with Ax_r^p and Bx_r^q dependences, respectively (Fig. 6). Then, for the whole diagram in Fig. 6,

$$\tilde{Q}'=\int_0^x dx_1\int_0^{x_1}dx_2\cdots\int_0^{x_{r-1}}dx_r ABx_r^{p+q}$$
$$=ABx_r^{p+q+r}\frac{(p+q)!}{(p+q+r)!} . \tag{13}$$

By using this rule repeatedly, one can obtain an expression for $\tilde{Q}$ for any diagram.

In order to derive (7) we have to know how to compute $d\tilde{Q}'_n/dx$. Since $\tilde{Q}'_n$ is always given by a power of x, this computation is trivial. What is less trivial is to put it into a form so that (7) can easily be derived. For that purpose let us consider Fig. 6 again. Since

$$\tilde{Q}'=ABx^{p+q+r}(p+q)!/(p+q+r)! ,$$

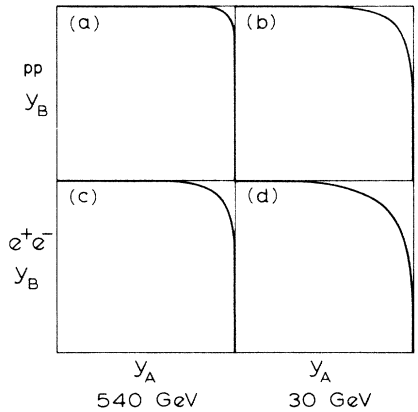

FIG. 5. Two-dimensional phase-space boundaries for pp and e^+e^- interactions at two energies. The y_A and y_B variables are linear functions of the x_A and x_B variables in the text normalized so that $(y_A,y_B)=(0,1)$ and (1,0) are points on the phase-space boundary.

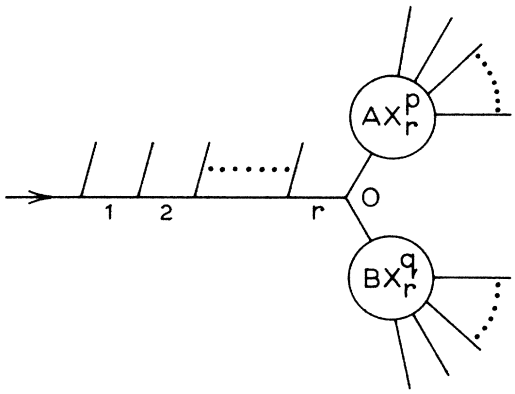

FIG. 6. A diagram used in deriving Eq. (13).

clearly

$$d\tilde{Q}'/dx = ABx^{p+q+r-1}(p+q)!/(p+q+r-1)!$$

$$=(p+q)ABx^{p+q+r-1}(p+q-1)!/(p+q+r-1)!.$$

Written in the latter form, we may interpret the action of d/dx to be the sum of two actions. One follows the upper branch and differentiates it at a point immediately after the branching at 0, and the other follows the lower branch and differentiates it at the same point. The differentiation on the upper branch turns Ax^p into pAx^{p-1}, resulting in a new diagram with

$$\tilde{Q}'=pABx^{p+q+r-1}(p+q-1)!/(p+q+r-1)! .$$

Similarly the differentiation on the lower branch yields a new diagram with a

$$\tilde{Q}'=qABx^{p+q+r-1}(p+q-1)!/(p+q+r-1)! .$$

If the upper branch consists of an on-shell particle, then $p=0$ and the d/dx action follows only the lower branch. If both branches are on-shell particles, then $p=q=0$ and the action stops. Thus the action of d/dx is like a current which follows the off-shell lines until it comes to the end, whence it removes the last vertex on that line from the diagram. In other words, the operator d/dx simply serves to remove the last vertices of the diagram one at a time in all possible ways.

Let us illustrate these results with Fig. 4. By using (13), one gets

$$\begin{aligned}&\tilde{Q}'_5(A)=x^3/2!1!, \quad \tilde{Q}'_5(B)=x^3/3! ,\\ &\tilde{Q}'_5(C)=x^3 2!/3!1!1! ,\\ &\tilde{Q}'_4(D)=x^2/1!1!, \quad \tilde{Q}'_4(E)=x^2/2! .\end{aligned} \tag{14}$$

Thus

$$\begin{aligned}&d\tilde{Q}'_5(A)/dx=\tilde{Q}'_4(D)+\tilde{Q}'_4(E) ,\\ &d\tilde{Q}'_5(B)/dx=\tilde{Q}'_4(E) ,\\ &d\tilde{Q}'_5(C)/dx=2\tilde{Q}'_4(E) .\end{aligned} \tag{15}$$

Equation (15) illustrates the rules of removing the last vertices. Removing the last vertices $a1$ and $a2$ in A yields D and E, respectively; removing b from B yields E and removing $c1$ and $c2$ from C yields E.

It remains to show that the symmetry factor F_S will cooperate with the d/dx action to yield (7). Before carrying out the general argument which is topological in nature, let us first see how this works in the special case of Fig. 4. The F_S for these diagrams have been given before. They are 4,2,8,8,2, for A,B,C,D,E. Therefore $\tilde{P}'_5(A)=\tilde{Q}'_5(A)/4$, $\tilde{P}'_4(D)=\tilde{Q}'_4(D)/8$, $\tilde{P}'_4(E)=\tilde{Q}'_4(E)/2$. We obtain, from (15),

$$d\tilde{P}'_5(A)/dx=2\tilde{P}'_4(D)+\tilde{P}'_4(E)/2 .$$

Similarly, we get

$$d\tilde{P}'_5(B)/dx=\tilde{P}'_4(E)$$

and

$$d\tilde{P}'_5(C)/dx=\tilde{P}'_4(E)/2 .$$

Adding these results, we get

$$\begin{aligned}d\tilde{P}_5/dx &= d[\tilde{P}'_5(A)+\tilde{P}'_5(B)+\tilde{P}'_5(C)]/dx\\ &=2[\tilde{P}'_4(D)+\tilde{P}'_4(E)]=4\tilde{P}_4/2 ,\end{aligned} \tag{16}$$

which agrees with Eq. (7).

To carry out the argument in general, note that the number of vertices in an n-particle diagram is $v=n-1$, and that the number of geometrically distinct diagrams corresponding to the same topological diagram is $2^v/F_S$. Thus $\tilde{P}_n=\tilde{Q}_n/F_S=2^{-(n-1)}$ (times the sum of $\tilde{Q}'_n$ for all geometrically distinct diagrams). Now d/dx acts on $\tilde{Q}'_n$ by removing the last vertices one at a time, thereby getting a number of diagrams with $n-1$ final particles. From an $n-1$ particle diagram, $n-1$ geometrically distinct n-particle diagrams can be created by adjoining a new vertex to each of the $n-1$ external lines. Conversely, the removal of this newly added vertex from each of these newly created geometrically distinct diagrams would yield back the original $n-1$ particle diagram. Thus (sum of $d\tilde{Q}'_n/dx$ for all geometrically distinct n particle diagrams)$=(n-1$ times the sum of $\tilde{Q}'_{n-1}$ of all the geometrically distinct $n-1$ particle diagrams). In other words

$$\frac{d}{dx}\tilde{P}_n=\tfrac{1}{2}(n-1)\tilde{P}_{n-1} \tag{17}$$

and Eq. (7) is finally proved.

It is also clear from these considerations that if only one source is present, as is the case in the multiperipheral chain of Fig. 1, then one may add a new vertex only to the source line and hence $d\tilde{P}_n/dx=\tilde{P}_n/2$.

The generalization beyond ϕ^3 vertices is easy. If the effective vertex is ϕ^{l+2}, then instead of the effective two-particle phase-space factor in (6) we must talk about an effective $(l+1)$-particle phase-space factor $\rho(S\to A_1A_2\cdots A_{l+1})$. We argue as in (6) that this can be taken as a function of m_s^2 only, and then we would proceed as before to introduce the wave-function factor and the function $x(m_s^2)$. The phase space at a vertex is now an $(l+1)$-dimensional hypercube if m_s^2 is large. The action of d/dx on $\tilde{Q}$ is still to remove the final vertices, but now this involves reducing l particles. Instead

of (7), we will therefore have

$$\frac{d}{dx}\tilde{P}_n=\tfrac{1}{2}(n-l)\tilde{P}_{n-l}\ . \tag{18}$$

The unitarized probabilities then satisfy the evolution equation

$$2\frac{d}{dx}P_n=(n-l)P_{n-l}-nP_n\ . \tag{19}$$

Note that we have chosen the normalization of x to yield the factor $\frac{1}{2}$ in (18). The relation between $x(s)$ and $\bar{n}(s)$ can be obtained from (19). It is $x=(2/l)\ln\bar{n}$.

This kind of generalization can also be made to the cases when we have a mixture of vertices of different l's, and to the case when more than one channel is present. In each case the evolution equation should be modified and the modification can be inferred simply from probabilistic considerations. See Sec. III for the case of a two-channel equation.

III. SOLUTIONS OF THE EVOLUTION EQUATIONS

A. One-channel evolution equation

If we have a mixture of vertices of different l, and if the wave-function factors are different l have the same energy dependence though not necessarily the same strength, then a formal solution to the evolution equation for this case

$$2\frac{dP_n}{dx}=\sum_{l\geq 1}\beta_l[(n-l)P_{n-l}-nP_n] \tag{20}$$

can be obtained. Here β_l are the relative strengths for the vertices ϕ^{l+2}. We shall normalize the definition of x such that $\sum_l\beta_l=1$. Then (20) implies $\bar{n}=\exp(\bar{l}x/2)$ where $\bar{l}=\sum_l l\beta_l$.

The generating function

$$P(\xi,x)=\sum_{n=-\infty}^{\infty}P_n(\bar{n}(x))\xi^n \tag{21}$$

(remember that $P_n=0$ for $n<0$) satisfies the equation

$$2\frac{\partial}{\partial x}P(\xi,x)=\sum_{l\geq 1}\beta_l\xi(\xi^l-1)\frac{\partial}{\partial\xi}P(\xi,x)$$

$$\equiv D_\xi P(\xi,x) \tag{22}$$

whose solution is given by

$$P(\xi,x)=\exp[\tfrac{1}{2}(x-x_0)D_\xi]P(\xi,x_0)\ . \tag{23}$$

Define the function $\eta(\xi)$ by

$$\frac{d\eta(\xi)}{d\xi}=\left[\sum_{l\geq 1}\beta_l\xi(\xi^l-1)\right]^{-1} \tag{24}$$

and denote its inverse function by $\xi=f(\eta)$. Then

$$P(\xi,x)=\exp\left[\tfrac{1}{2}(x-x_0)\frac{\partial}{\partial\eta}\right]P(f(\eta),x_0)$$

$$=P(f(\eta(\xi)+\tfrac{1}{2}(x-x_0)),x_0)\ . \tag{25}$$

In principle, $P_n(x)$ can be read out from (25) by expanding it in powers of ξ.

In practice it is not so easy to obtain $\eta(\xi)$ and $f(\eta)$ analytically. It is also not simple to do the power-series expansion in ξ. However, when we have vertices with a fixed l, then the solution can indeed be obtained.[11] In that case,

$$\frac{d\eta(\xi)}{d\xi}=[\xi(\xi^l-1)]^{-1}$$

and this can be solved by letting $\xi'=\xi^l$. Then we obtain

$$l\eta=\ln\frac{\xi^l-1}{\xi^l}$$

and

$$\xi=f(\eta)=(1-e^{l\eta})^{-1/l}\ .$$

Consequently,

$$f(\eta+\tfrac{1}{2}(x-x_0))=\xi\Big/\left[\left[1-\frac{\bar{n}}{\bar{n}_0}\right]\xi^l+\frac{\bar{n}}{\bar{n}_0}\right]^{1/l}, \tag{26}$$

where

$$\bar{n}_0\equiv\bar{n}(x_0)\ .$$

Now define G_n^k by

$$f^k=\sum_n G_n^k(w)\xi^n\ , \tag{27}$$

where $w=\bar{n}/\bar{n}_0$. Then

$$G_n^k(w)=\sum_p w^{-k'}\frac{\Gamma(k'+p)}{\Gamma(k')\Gamma(p+1)}\left[1-\frac{1}{w}\right]^p\delta_{n,k+lp}\ , \tag{28}$$

where $k'\equiv k/l$. In the KNO limit when $n\gg 1$, $\bar{n}\gg 1$, and $z=n/\bar{n}$ fixed,

$$G_n^k\to\frac{\bar{n}_0}{\bar{n}}\left[\frac{z\bar{n}_0}{l}\right]^{k'-1}\frac{1}{(k'-1)!}e^{-(\bar{n}_0/l)z}\ . \tag{29}$$

The solution of the evolution equation with the initial distribution $P_n(x_0)=\alpha_n$ is

$$P_n(x)=\sum_{k\geq 1}\alpha_k G_n^k\left[\frac{\bar{n}}{\bar{n}_0}\right]\ . \tag{30}$$

We can think of this as the multiplicity distribution resulting from the decay of k clusters produced initially by the collision, and that α_k gives the distribution for producing these k clusters. The number $\bar{n}_0=\sum_n n\alpha_n$ is then the average number of the initial clusters. It is useful to note that in the KNO limit, if $\alpha_n=\delta_{nk}$, then the pth moment of z is given by

$$\langle z^p\rangle=\left[1+\frac{1}{k'}\right]\left[1+\frac{2}{k'}\right]\cdots\left[1+\frac{p-1}{k'}\right]\ . \tag{31}$$

Note that for finite energies (28) is not identical to (29). This model therefore naturally contains KNO-scaling violations. Strictly speaking these are not really violations; we simply have not yet reached the scaling limit at lower energies. Another source of scaling violations of kinematical origin was discussed in Sec. II: the evolution

equation is valid only at high energies. At lower energies the region of phase space as depicted in Fig. 5 is not a square and the nonzero on-shell masses must also be accounted for. These considerations have the effect of making the multiplicity distributions narrower (more Poisson-type) and more symmetrical about $z=1$ (i.e., the long tail at large z has been cut off by the loss of large multiplicity events).

B. A two-channel problem

Consider a two-channel problem and refer to the particles in the two channels as gluons and quarks. We assume that there are three kinds of interactions, as depicted in Fig. 7. We emphasize that despite the terminology, we are not necessarily considering real quarks and gluons. They could be any two kinds of particles coupled in the way shown in Fig. 7. We also point out that spin and other complications have not been built into this model so that these quarks and gluons are spinless. Nevertheless, if their coupling were determined by the usual SU(3)-color factors for real gluons and quarks, then $A:B:C=4/3:F/2:3$, where F is the number of quark flavors. The sudden opening up of a new flavor threshold will change B, and hence, the evolution equation, and therefore will lead to KNO scaling violations.

The evolution equation is

$$\frac{d}{dx}P(n,m)=A[nP(n,m-1)-nP(n,m)] +B[(m+1)P(n-2,m+1)-mP(n,m)] +C[(m-1)P(n,m-1)-mP(n,m)] , \quad (32)$$

where $P(n,m)$ is the probability of finding m gluons and n quarks or antiquarks. This equation is difficult to solve analytically, except in some special situations. We will now discuss them individually.

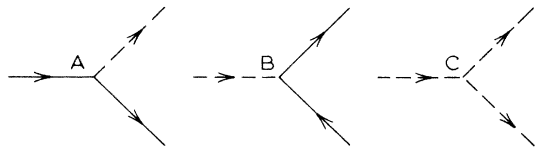

FIG. 7. The three basic vertices for the two-channel model considered in Sec. III.

(i) We can easily obtain from (32) the equation for the moments. For the first moments, they are

$$d\bar{n}/dx=2B\bar{m}, \quad d\bar{m}/dx=A\bar{n}+(C-B)\bar{m} . \quad (33)$$

Assuming an initial condition of $m=1$ and $n=0$ at $x=0$, the solution of (33) is

$$\bar{n}(x)=\frac{2B}{E}(e^{\lambda x}-e^{\mu x}) , \quad \bar{m}(x)=\frac{1}{E}(\lambda e^{\lambda x}-\mu e^{\mu x}) , \quad \lambda,\mu=\tfrac{1}{2}[D\pm E], \quad D=C-B , \quad E=(D^2+8AB)^{1/2} . \quad (34)$$

For large x, the larger eigenvalue λ dominates the energy variation. Then $\bar{n}/\bar{m}$ is a constant. Similarly, it can be shown from the moment equations for any initial conditions that

$$\frac{\langle n^a m^b\rangle}{\bar{n}^a\bar{m}^b}=R_{a+b}, \quad \frac{\langle n^a m^b\rangle}{\langle n^{a-1}m^{b+1}\rangle}=\frac{2B}{\lambda} , \quad (35)$$

where R_{a+b} is independent of energy. Thus KNO scaling is valid in this limit. The second-moment equations are

$$d\langle n^2\rangle/dx=4B(\langle nm\rangle+\bar{m}), \quad d\langle nm\rangle/dx=A\langle n^2\rangle+B(2\langle m^2\rangle-2\bar{m}-\langle nm\rangle)+C\langle nm\rangle , \quad d\langle m^2\rangle/dx=A(2\langle nm\rangle+\bar{n})+B(-2\langle m^2\rangle+\bar{m})+C(2\langle m^2\rangle+\bar{m}) . \quad (36)$$

The solution of this is contained in (36), and a rather lengthy calculation for the initial conditions previously specified leads to the result

$$R_2=2\{D(2A-C)(\lambda+2\mu)+2[3AB(A+C)+D^2(C-A)]\}/\lambda(D^2+9AB) . \quad (37)$$

(ii) $B=0$. In this case the quark number n is conserved. Gluons are emitted from quarks by A and from gluons by C. If $C=0$, then the solution is a Poisson distribution, and it is narrow. From now on we shall assume $C\neq 0$. With $B=0$ this problem has become a one-channel problem and the technique used in case A is still applicable in this case. If we start with k gluon clusters, the result in the KNO limit is a γ distribution with an exponential slope $k'=k+Q$, where $Q=An/C$. Thus even if k' is known from data fitting, we cannot know what the number k of initial gluon clusters is, especially if Q turns out to be a large number.

(iii) $A=0$. The evolution equation for $P_m=\sum_n P(n,m)$ is

$$dP_m/dx=B[(m+1)P_{m+1}-mP_m] +C[(m-1)P_{m-1}-mP_m] . \quad (38)$$

This differs from the one-channel equation by having the B term present. This term describes the disappearance of gluons when a quark pair is produced. We will therefore find that if we start with k clusters, we may now get $n<k$ particles at larger x, a phenomenon that never occurs in the one-channel case.

Multiplying both sides of (38) by m and summing over m, we obtain an equation for the average multiplicity

which can be solved to yield $\overline{m}=\overline{m}_0\exp(Dx)$, where $D=C-B$. Thus if $C<B$, the average multiplicity decreases with energy. This is because the production of gluons from the C term cannot catch up with the loss of gluons from the B term. Suppose now $C>B$ and $D>0$. Then $\rho\equiv B/C<1$. Equation (38) can be solved with the same technique as in the one-channel case. Using the notation there, we find

$$P(\xi,x)=P(f(\eta(\xi)+Cx),0)\ ,$$
$$f(\eta(\xi)+Cx)=(\alpha\xi-\rho\gamma)/(\gamma\xi-\delta)\ , \tag{39}$$
$$\alpha=\rho\overline{m}/\overline{m}_0-1,\quad \gamma=\overline{m}/\overline{m}_0-1,\quad \delta=\overline{m}/\overline{m}_0-\rho\ .$$

There is no problem in obtaining a general solution from (39) for any initial condition, but it is sufficient to take the simple case when $P_m=\delta_{m1}$ initially at $x=0$ to illustrate the new features for this reaction. In that case $\overline{m}_0=1$, and the probability in the KNO limit is

$$P_m=\frac{1}{\overline{m}}\{\rho\delta(z)+(\rho-1)^2\exp[-(1-\rho)z]\}\ ,$$
$$z=m/\overline{m}\ . \tag{40}$$

The emergence of the δ function and the associated change of exponential slope is the new feature in this reaction. It is caused by the loss term B which results in a piling up of particles at $z=0$. Then change of the exponential slope from 1 in the one-channel case to $1-\rho$ in this case is then necessary to maintain the sum rule that the zeroth and the first moments of a KNO function must both be 1.

IV. PHENOMENOLOGICAL APPLICATIONS

In this section we shall apply the one-channel analysis to hadron-hadron multiplicity distributions. A multichannel analysis would have been needed to calculate the simultaneous multiplicity distribution of pions and kaons (or some other types of hadrons), but no experimental data on these joint distribution are presently available.

We will concentrate on a one-channel analysis. In such a system the wave function (form-factor-propagator combination) is determined by the average multiplicity and can therefore be considered as known. The dynamics is then solely controlled by l ($l=1,2,3,\ldots$), where $l+1$ is the number of lines emerging to the right of a vertex. Again for the sake of simplicity we will assume to have only one kind of vertex with a fixed l and we will proceed to discuss the experimental data in this framework.

Under this framework it was shown in Sec. III [Eq. (30)] that the final multiplicity distributions P_n are given by the initial-cluster distributions α_k as

$$P_n(x)=\sum_{k\geq 1}\alpha_k G_n^k\left[\frac{\overline{n}}{\overline{n}_0}\right]\ . \tag{41}$$

It is known that up to CERN ISR energies the multiplicity distributions for all hadron-hadron reactions satisfy KNO scaling quite well and that the KNO curve common to all reactions can be parametrized, e.g., by the Slattery distribution.[13] From ISR to S$\bar{p}p$S energy of $\sqrt{s}=540$ GeV, violations of KNO scaling become apparent.

It has been shown by Carruthers and Shih[6] that throughout the whole energy range from Fermilab to S$\bar{p}p$S energies, the multiplicity distribution can be fitted very well if leading particles are subtracted.

Our distribution given in (28) and (29) is different from theirs and gives rise to as good an agreement as theirs when we take $k'=3$ (see Fig. 8). If we want a perfect fit then additional energy violations of k' is necessary.[14] Whether this can be accounted for by the kinematical corrections discussed in this paper remains to be seen.

There remains the question of what l is. If the channel in question is taken to involve pions, the G-parity conservation would forbid $l=1$. If we take $l=2$, then the initial cluster number would be $k=6$. Why this number is so large is presently not understood, but perhaps we should not attribute too much significance to it at this point. The number of clusters depends critically on the dynamics involved (e.g., the number l), and a multichannel analysis (see, e.g., the example in Sec. III) is capable of reducing the number of clusters. It is also possible that the good agreement with data from a one-channel analysis is coincidental.

We have emphasized how naturally KNO scaling arises in the MPSM for kinematical reasons. This does not mean that KNO-scaling violations will not occur dynamically. The simplest mechanism of that type is to have k, the number of the initial clusters, vary with energy. This, in spirit at least, is analogous to the way how KNO violations are explained in the three-fireball model. There is another more interesting way how KNO-scaling violation can occur in our model. If the underlying dynamics is altered by the opening up of an important channel (see the

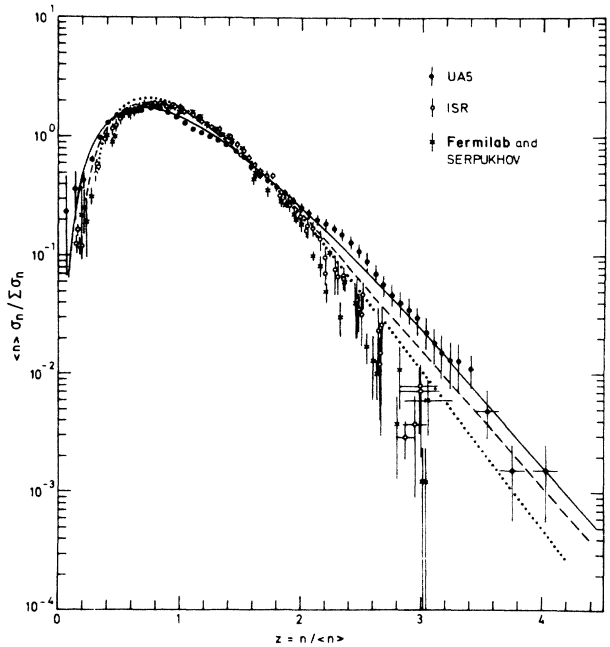

FIG. 8. Multiplicity distributions for pp and $\bar{p}p$ reactions. Data have been taken from Ref. 5 and the sources quoted therein. The theoretical results are obtained from (28) by taking $k'=3$. The average multiplicities $\overline{n}$ used for the solid, dashed, and dotted curves are, respectively, 29.1 (S$\bar{p}p$S), 12 (ISR), and 8.5 (Fermilab).

discussion in Sec. II for an example when the flavor number F changes), or more dramatic still, by the complete alteration of the underlying dynamics. One might imagine that ordinarily, some sort of hadronic tree diagrams would be sufficient to explain the observed multiplicity distributions. But if a deconfining phase transition occurs, then surely we have to use quarks and gluons and QCD to describe the dynamics afterward. This sudden alteration of the dynamics changes the evolution equation for P_n and hence causes a scaling violation. For this reason multiplicity distributions may be a good tool to provide a signature for the detection of a deconfining transition in heavy-ion collisions.

ACKNOWLEDGMENTS

C.S.L. wishes to thank P. Hoyer, R. C. Hwa, and C. N. Yang for stimulating discussions. This work was supported in part by the Natural Sciences and Engineering Research Council of Canada and the Quebec Department of Education.

[1]Z. Koba, H. B. Nielsen, and P. Olesen, Nucl. Phys. **B40**, 317 (1972).

[2]A. Firestone *et al.*, Phys. Rev. D **14**, 2902 (1976); D. Fong *et al.*, Nucl. Phys. **B102**, 386 (1976); A. E. Brenner *et al.*, Phys. Rev. D **26**, 1497 (1982); D. Brick *et al.*, *ibid.* **25**, 2794 (1982); W. Thomé *et al.*, Nucl. Phys. **B129**, 365 (1977); A. Breakstone *et al.*, Phys Rev. D **30**, 528 (1984).

[3]Ch. Berger *et al.*, Phys. Lett. **95B**, 313 (1980).

[4]R. L. Cool, K. Goulianos, S. L. Segler, H. Sticker, and S. N. White, Phys. Rev. Lett. **48**, 1451 (1982).

[5]G. J. Alner *et al.*, Phys. Lett. **138B**, 304 (1984); UA5 Collaboration, G. J. Alner *et al.* (unpublished).

[6]P. Carruthers and C. C. Shih, Phys. Lett. **127B**, 242 (1983); **137B**, 425 (1984).

[7]A. Capella and J. Tran Thanh Van, Phys. Lett. **114B**, 450 (1982); A. B. Kaidalov and K. A. Ter-Martirosyan, *ibid.* **117B**, 247 (1982); P. Aurenche and F. W. Bopp, *ibid.* **114B**, 363 (1982).

[8]M. LeBellac, J. L. Meunier, and G. Plaut, Nucl. Phys. **B62**, 350 (1973); T. T. Chou and C. N. Yang, Phys. Lett. **116B**, 301 (1982); **135B**, 175 (1984); C. S. Lam and P. Yeung, *ibid.* **119B**, 445 (1982); Phys. Rev. D **28**, 1213 (1983); S. Barshay, Phys. Lett. **116B**, 193 (1980).

[9]C. Hayot and G. Sterman, Phys. Lett. **121B**, 419 (1983); G. Pancheri and Y. N. Srivastava, *ibid.* **128B**, 433 (1983).

[10]Chou Kuang-Chao, Liu Lian-sou, and Meng Ta-chung, Phys. Rev. D **28**, 1080 (1983); Liu Lian-sou and Meng Ta-chung, *ibid.* **27**, 2640 (1983).

[11]C. S. Lam and M. A. Walton, Phys. Lett. **140B**, 246 (1984).

[12]P. Cvitanovič, P. Hoyer, and K. Konishi, Phys. Lett. **85B**, 413 (1979); P. Cvitanovič, P. Hoyer, and K. Zalewski, Nucl. Phys. **B176**, 429 (1980); A. D'Innocenzo, G. Ingrosso, and P. Rotelli, Nuovo Cimento **A25**, 393 (1979); **A55**, 417 (1980).

[13]P. Slattery, Phys. Rev. D **7**, 2073 (1973).

[14]Recent data show that if we separate the events into jet and nonjet, then the KNO distributions of each have little energy variation. In particular, the nonjet part can be fitted with $k'=3$ much better than Fig. 8 because of its small energy variations.